PAPER

Check for updates

Magnetic few-layer graphene nanocomposites for the highly efficient removal of benzo(*a*)pyrene from water†

Joana Vaz-Ramos,[ab] Dominique Bégin,[b] Paula Duenas-Ramirez,[a] Anaïs Becker,[b] Mathieu Galmiche,[b] Maurice Millet,[b] Sylvie Bégin-Colin [iD] *[a] and Stéphane Le Calvé [iD] *[b]

Regarding the importance of water pollution by persistent organic pollutants and the need for innovative processes to extract them efficiently, we designed magnetic few-layer graphene-based composite nanomaterials (CNs) for high removal from water of a particularly toxic polycyclic aromatic hydrocarbon (PAH): benzo(*a*)pyrene (BaP). The CNs were prepared in a one-step polyol solvothermal synthesis process by introducing few-layer graphene coated with tannic acid in the reaction medium of iron oxide nanostructures. The synthesis was reproducible and allowed obtaining a large amount of magnetic CNs, which can be easily and quickly magnetically removed from aqueous medium. BaP adsorption on CNs was studied for an initial BaP aqueous concentration of 1–5000 μg L^{-1}. A very low amount of CNs (5 mg L^{-1}) was sufficient and effective to have a very high and fast BaP adsorption in comparison with previous studies reporting an adsorbent amount of 5–1000 mg L^{-1}. Removal efficiencies of 99.95 ± 0.01% in water with 1% ethanol as co-solvent were reached in minutes. The presence of iron oxide was observed to not affect the adsorption capacity of CNs. The volume percentage of ethanol in the water media influenced the removal efficiency of BaP by the CNs. With 50 vol% ethanol necessary to obtain an adsorption isotherm, the adsorption follows Langmuir's law with a maximum adsorption capacity q_{max} = 69.45 ± 5.20 mg g^{-1} and a Langmuir isotherm constant K_L = 1.92 ± 0.54 L mg^{-1}. These CNs, compared with other BaP and PAH adsorbents, are clearly very promising for BaP removal from polluted media.

Environmental significance

Anthropogenic pollution leads to the presence of many organic pollutants in water. Polycyclic aromatic hydrocarbons (PAHs) are toxic, mutagenic, and carcinogenic, so their removal from polluted environments is essential, particularly benzo(*a*)pyrene (BaP), a highly carcinogenic PAH. Here, we designed magnetic graphene composite nanomaterials (CNs) for the adsorption of this problematic pollutant. The synthesized CNs showed up to 99.95% BaP removal from water, coupling very efficient and fast adsorption with easy magnetic recovery of the adsorbent. The development of such a highly efficient adsorbent means that only small adsorbent amounts are needed for depollution practices. Furthermore, these CNs could have potential for the removal of other PAHs and pollutants and could thus have a positive impact on environmental depollution techniques.

1. Introduction

As the world population continues to grow and industrialization increases, there is both an increase on the demand for clean water and an increase in water pollution.[1,2]

[a] *Institut de Physique et Chimie des Matériaux de Strasbourg (IPCMS), UMR-7504 CNRS-Université de Strasbourg, 23 rue du Lœss, 67034 Strasbourg Cedex 2, France. E-mail: sylvie.begin@unistra.fr*

[b] *Institut de Chimie et Procédés pour l'Energie, l'Environnement et la Santé (ICPEES), UMR-7515 CNRS-Université de Strasbourg, 25 rue Becquerel, 67087 Strasbourg, France. E-mail: slecalve@unistra.fr*

† Electronic supplementary information (ESI) available. See DOI: https://doi.org/10.1039/d3en00047h

Over 30% of the world population does not have access to clean water and there is a continuous growing pressure on fresh water supplies.[3] A lot of different pollutants exist in water, both organic and inorganic, that mostly originate from human activities, such as industrial and domestic effluents, wastewater from agricultural activities, *etc.*[3,4] These pollutants can be harmful to human health as well as to aquatic life and ecosystems,[5] so monitoring their presence and removing them from water bodies are crucial.

Polycyclic aromatic hydrocarbons (PAHs) are a particularly important family of organic pollutants because they are ubiquitous pollutants in the environment, in water,[6] air,[7] and soil.[8] PAHs are organic compounds with two or more fused

1660 | *Environ. Sci.: Nano*, 2023, **10**, 1660–1675

This journal is © The Royal Society of Chemistry 2023

aromatic rings in their chemical structure. They are mostly produced by anthropogenic sources, mainly from the incomplete combustion of organic materials, in different activities such as residential heating, vehicular emissions and industries.[6,9,10] However, they can also originate naturally from volcanic eruptions and forest fires.[6,10] PAHs are introduced in the environment mostly by emission into the atmosphere, where they are usually bound with particulate matter[11–13] depending on their vapor pressures. They can also further deposit into water bodies, soils and vegetation by dry and wet deposition.[6] Furthermore, they can also directly enter water bodies in wastewater effluents.[10,14] PAHs have associated health risks; namely, they are mutagenic, carcinogenic, toxic and endocrine disruptors,[15] and thus their removal from polluted environments is of utmost importance. Hundreds of PAHs have been identified to this day, but only sixteen PAH compounds are considered as priority control pollutants by the United States Environmental Protection Agency (US EPA). Among them, benzo(a)pyrene (BaP) is highly carcinogenic, and thus it is considered as the reference PAH for carcinogenicity. In order to limit human exposure to PAHs, the European Union, for example, has established a target maximum concentration of 0.100 µg L^{-1} in drinking water for total PAHs, in general, and, in particular, 0.010 µg L^{-1} for BaP.[16]

Considering the strong necessity of removing such toxic pollutants from water, there has been a great interest in developing efficient methodologies for this purpose over the past decades. A wide range of different techniques of water depollution have been investigated, such as precipitation, membrane processes, extraction, coagulation and adsorption.[3,4,17] Most of them have associated limitations, like high operational costs, limited efficiency, or complex design.[3] Adsorption processes have gained more and more attention due to their lower cost, simpler design, and capability to remove in an efficient way various pollutants including organic and inorganic ones. In adsorption processes, the pollutant molecules in water interact and get attached to the surface of a solid material (called adsorbent) and are then removed from solution.[3,17] A lot of different materials can be used as adsorbents, allowing the removal of different pollutants, but there is always a strong need for new adsorbent materials in order to provide viable and effective depollution processes with adsorbents that are low-cost, easily removed from polluted media and ideally also recyclable.[3] In recent years, a lot of attention has been paid to nanomaterials for depollution applications because they display a high surface area,[18] providing a high contact surface with the pollutant molecules and thus making them attractive for adsorption applications. Among promising nano-sized adsorbents, graphene and graphene-based materials are well known to be highly efficient adsorbents of organic pollutants due to π–π stacking interactions between the aromatic rings of graphene and the unsaturated organic pollutant molecules including the aromatics. However, further separation from water of these nanomaterials doped

with organic species after adsorption can be hazardous and difficult. One possible strategy to overcome this hard separation is the use of magnetic nanomaterials, such as iron oxide, because their magnetism could allow an easy magnetic separation of the adsorbent materials,[19] decreasing the risk of contamination of the treated water with residual adsorbent. The possibility to create composite nanomaterials (CNs) that couple the high adsorption efficiency of graphene nanomaterials with the easy magnetic separation (due to anchored magnetic nanomaterials on graphene sheets) is highly attractive to develop effective strategies for water decontamination, allowing water recyclability and reuse.

Adsorption with carbon-based and/or magnetic nanomaterials has already been studied for the removal of PAHs from water as well as other pollutants such as pesticides,[20,21] phenolic compounds,[22,23] and PCBs.[24,25] The adsorption of PAHs with these nanomaterials has shown promising results in the literature (Table S1†).[19,26–32] Indeed, for example, graphene wool materials have already been used for the adsorption of PAHs, showing removal efficiencies between 52.2% and 100% depending on the amount of adsorbent and on the studied PAH,[32] confirming the efficiency of graphene-based materials in PAH removal. Moreover, Zhang et al. used CNs of carbon nanotubes/ nanosheets and magnetic nanoparticles for the adsorption of phenanthrene, reaching removal efficiencies of 100%, and thus showing the potential of magnetic carbon CNs for this application.[19] However, the problems to face with graphene are the poor suspension stability of graphene sheets in hydrophilic medium and their tendency to stick together, limiting their performance. We developed the production of few-layer graphene (FLG) coated with tannic acid (TA),[33] ensuring a high suspension stability of FLG in hydrophilic medium. In addition, the anchoring of magnetic iron oxide nanostructures at the FLG surface would ensure a good separation and high surface accessibility of FLG.[34,35]

Due to the high carcinogenicity of BaP, it is particularly important to remove this specific compound from polluted waters. To the best of our knowledge, no studies were found in the literature where magnetic graphene-based CNs were used for the adsorption of BaP from water. Therefore, in this work, we developed magnetic graphene-based CNs, constituted of few-layer graphene coated with tannic acid (FLG@TA) and iron oxide raspberry-shaped nanostructures (RSNs)[36,37] for the removal of BaP from water. As explained above, the presence of tannic acid around graphene layers ensures the stability of graphene in water as well as the separation between layers, allowing a high amount of surface available for adsorption of the pollutant. On the other hand, we chose iron oxide RSNs because they consist in aggregates of oriented nanograins with a magnetite phase composition, which provides them a high magnetization, despite the small size of the nanograins, and a superparamagnetic behavior.[36,37] Indeed, this superparamagnetism makes these RSNs nonmagnetic in the absence of a magnetic field and they magnetize only under the application of a magnetic

This journal is © The Royal Society of Chemistry 2023

Environ. Sci.: Nano, 2023, 10, 1660–1675 | 1661

field. Thus, RSNs do not tend to aggregate in suspension due to harmful magnetic interactions. Therefore, RSNs are highly magnetic, which allows easy magnetic separation of CNs once adsorption is performed, and also ensure a good separation of graphene layers. One may notice that in earlier studies iron oxide–graphene CNs were produced with graphene without tannic acid coating, and thus the nanocomposites combining FLG, iron oxide nanostructures and tannic acid are quite new and most importantly form stable aqueous suspensions. The aim of this work was first to design such a nanocomposite that combines magnetic separation with high removal of BaP and then to study the adsorption of BaP using a very small quantity of CNs (5 mg L^{-1}) and by varying the initial BaP concentration as well as the adsorption time. To the best of our knowledge, no work in the literature has used such a small amount of graphene-based adsorbents for efficient adsorption of BaP in water.

2. Experimental section

2.1. Materials

Expanded graphite (MERSEN France), tannic acid (C$_{76}$H$_{52}$O$_{46}$, Sigma Aldrich), iron(III) chloride hexahydrate (FeCl$_3\cdot$6H$_2$O, >99%, Sigma Aldrich), succinic acid ((CH$_2$)$_2$(CO$_2$H)$_2$, >99.5%, Sigma Aldrich), urea (CO(NH$_2$)$_2$, 99.3+%, Alfa Aesar), ethylene glycol ((CH$_2$OH)$_2$, 99%, Thermo Scientific), benzo(a)pyrene (C$_{20}$H$_{12}$, 96.5%, Acros Organics) and acetonitrile (CH$_3$CN, ≥99.9%, CHROMASOLV™ Gradient, for HPLC, Honeywell Riedel-de Haën™) were used as received. Deionised water was used for the synthesis and for adsorption experiments.

Methanol (CH$_3$OH, HiPerSolv CHROMANORM®, for HPLC – isocratic grade) and water (CHROMASOLV™ Plus, for HPLC, Honeywell Riedel-de Haën™) were used as the mobile phase for liquid chromatography.

2.2. Synthesis of few-layer graphene coated with tannic acid (FLG@TA)

FLG@TA was prepared by a top-down approach from expanded graphite.[33] Briefly, expanded graphite (500 mg) and tannic acid (250 mg) were added to water (500 mL) in a 1000 mL glass beaker containing a magnetic stirrer. The mixture was placed under ultrasounds for 4 h at a continuous pulse of 25% of the maximum frequency using a Branson 450 Digital Sonifier (400 W, 20 kHz) and under simultaneous magnetic stirring. Furthermore, the glass beaker was immersed in a thermostatic bath at room temperature during this process to limit the temperature increase caused by the sonication process. The ultrasounds separated the graphene layers and tannic acid acted as a surfactant, stabilizing the separated layers and preventing their restacking. Indeed, due to the specific structure of TA, its aromatic rings can conjugate with the aromatic structure of graphene layers by π–π stacking. Furthermore the presence of many hydroxyl and phenolic groups in TA favors an optimal dispersion in an aqueous medium as well described by Yu et al.[38] and by Zhao et al.[39] A colloidal suspension of FLG@TA in water was thus

obtained. An illustration of this step of the synthesis is given in Fig. S1.†

2.3. Synthesis of FLG@TA@RSN composite nanomaterials

The FLG@TA@RSN composites were prepared by a modified solvothermal polyol method where FLG@TA was added to the reaction medium of a typical RSN synthesis following a previously established method.[35] Nevertheless, one may notice that this previous synthesis method was conducted with FLG uncoated with tannic acid and so the impact of tannic acid on the composite synthesis will be studied here.

First, the suspension of FLG@TA was freeze-dried overnight after freezing by liquid nitrogen using an Alpha 2–4 LD lyophilizer from Christ. Then, the freeze-dried FLG@TA (300 mg) was dispersed in ethylene glycol (60 mL) and placed under magnetic stirring for at least one day to ensure complete homogeneous dispersion of the FLG@TA in ethylene glycol. FeCl$_3\cdot$6H$_2$O (1.63 g), succinic acid (0.24 g) and urea (3.6 g) were then added to the mixture, which was placed under magnetic stirring for 2 h followed by 1 h under sonication in an ultrasound bath. The reaction mixture was then sealed in a stainless-steel autoclave lined with an inner Teflon reactor (capacity of 75 mL) and placed inside an oven. The reaction mixture was slowly heated to 200 °C at 1.5 °C min^{-1} and left at this temperature for 10 h 30 min before being cooled to room temperature inside the oven. The synthesized materials were then separated magnetically and washed 9 times with a mixture of 50% ethanol/50% acetone (4 min in the ultrasound bath). After washing, the FLG@TA@RSNs were stored in ethanol until further characterization or use.

2.4. Characterization of the synthesized materials

Fourier transform infrared (FTIR) spectroscopy was used to identify the chemical groups present in FLG@TA and in the FLG@TA@RSN composites. The IR spectra were recorded in a Perkin Elmer Spectrum 100 spectrometer for wavenumbers between 4000 and 400 cm^{-1}. For the preparation of the samples, a few drops of the suspension of composites in ethanol were mixed with dry KBr and after the evaporation of the solvent, pellets were prepared and FTIR transmittance spectra were obtained.

X-ray diffraction (XRD) was used to identify the crystalline phases present. The X-ray diffractometer was a Bruker D8 Discover equipped with a Lynx-Eye detector in the 20–70° (2θ) range with a scan step of 0.03° and the sample rotated at 30 rpm during the measurement. Silicon powder was used as internal standard. The diffraction peaks were compared to the JCPDS database. Profile matching with the software Fullprof was used to obtain estimates of the crystallite size and lattice parameter.

Scanning electronic microscopy (SEM) was used to obtain images of the synthesized composites using a Zeiss Gemini SEM 500 electron microscope operating at 3.00 kV. The FLG@TA@RSN composites were deposited on silicon wafers and posteriorly observed by SEM.

Transmission electronic microscopy (TEM) was performed to obtain images of the synthesized materials. For this, a Topcon 002B high-resolution transmission electron microscope operating at 200 kV was used. The samples were deposited on carbon-coated copper grids. After the image acquisition, the software ImageJ was used to obtain the size distribution of the iron oxide nanostructures in the composites.

Thermogravimetric analysis (TGA) was performed on an SDT 600 analyzer from TA Instruments to measure the mass loss of the sample when the temperature changed. The measurements were performed under an air flow from room temperature to 900 °C at a heating rate of 5 °C min⁻¹. The composite was previously dried before analysis.

Electrophoretic mobility experiments were performed to study the zeta potential of FLG@TA@RSN suspensions in water and determine the isoelectric point using a Zetasizer Nano ZS analyzer from Malvern Panalytical. The zeta potential measurements were performed at 25 °C. The composites were suspended in water under very dilute conditions to obtain suspensions with low turbidity (but leading to a count rate of >50 kcps during the measurements) and sonicated for 10 min prior to analysis. The pH was adjusted with HCl (0.1 M) and NaOH (0.1 M) solutions. The measurements were checked at the end to make sure they met quality criteria given automatically by the equipment.

The specific surface area was determined by nitrogen adsorption–desorption isotherms using the BET method with Tristar equipment from Micromeritics. Prior to analysis, the sample was degassed under vacuum at 150 °C.

2.5. Adsorption experiments of benzo(*a*)pyrene

As pointed out in the introduction, benzo(*a*)pyrene was selected among PAHs as a pollutant of interest due to its high carcinogenicity. Batch adsorption experiments were performed to study the adsorption process. Adsorption experiments were performed at room temperature, using FLG@TA@RSN as adsorbent at a fixed concentration (5 mg L⁻¹). The concentration of the composite for the adsorption experiments was determined in preliminary experiments based on the concentration values reported in the literature (see references in Table S1†). For higher concentrations of composite, namely 50 mg L⁻¹, no BaP was detected by UHPLC-FLD after adsorption, which limited the study of the adsorption process. Therefore, the concentration was reduced to 5 mg L⁻¹ composite, for which preliminary results showed the presence of residual BaP after adsorption.

Due to its low water solubility, a parent solution of BaP (100 mg L⁻¹) was prepared in ethanol to ensure complete solubilization and this solution was diluted daily into working solutions for the adsorption experiments. Previous studies by Qian *et al.* had shown that treated glass could adsorb benzo(*a*)pyrene even in the presence of a co-solvent,[40] so different percentages of ethanol (1%, 10% and 50%) were used during the adsorption experiments to consider this effect as well as to study the influence of ethanol in the adsorption process. 1% ethanol was chosen for the experiments to be in close conditions to pure water experiments while ensuring the solubility of BaP, and 50% was chosen because, for the isotherm studies, much higher concentrations of BaP were needed. Hence this percentage of ethanol ensured that BaP was solubilized.

To study the kinetics, adsorption times between 30 s and 1 h were considered. For the adsorption isotherms, the established adsorption time was 1 h to ensure that the adsorption reached equilibrium. Concentrations of BaP between 1 and 10 μg L⁻¹ were used for experiments with 1% ethanol, while concentrations of 10 μg L⁻¹ up to 5000 μg L⁻¹ were used for experiments with 50% ethanol. The effect of the amount of ethanol was also evaluated at 10 vol% with a BaP concentration of 10 μg L⁻¹.

Briefly, in the adsorption experiments, dried adsorbent materials were dispersed in ultrapure water (60 mL, 20 mg L⁻¹) in 96.5 mL clear glass flasks and sonicated for 10 min. Fresh suspensions of adsorbent were prepared for every group of experiments. Then, in 20 mL glass volumetric flasks, the BaP solution and ethanol were mixed before adding the adsorbent suspension (5 mL) and water to complete the total volume (20 mL). The flasks were closed and placed in a mechanical stirrer for a certain adsorption time. Afterwards, the adsorbent FLG@TA@RSN was magnetically separated, and the supernatant was filtered with a 0.20 μm syringe filter (Chromafil Xtra PA-20/25) and stored in 40 mL clear glass vials with closed-top caps until quantification. Before quantification, a small volume of the samples to be analyzed (1 mL) was transferred to 2 mL R.A.M.™ (9 mm) clear glass vials from Supelco.

In addition to the abovementioned FLG@TA@RSN sorption experiments, adsorption experiments using FLG@TA as adsorbent (without RSNs) were also performed to assess if the presence of iron oxide had a negative effect on BaP adsorption. The experiments were performed in 50% ethanol with a concentration of 10, 500 and 3000 μg L⁻¹ BaP.

In the case of FLG@TA, since this material is not magnetic, only filtration with a syringe filter was performed. Filtration was performed two times to ensure all the adsorbent was removed from the supernatant.

After the determination of the concentration of BaP in solution (see section 2.6), the adsorption capacity (q_E) and removal efficiency (RE) were calculated by the following equations:

$$q_E = \frac{(C_0 - C_E)V}{m_{ads}} \tag{1}$$

$$RE = \frac{C_0 - C_E}{C_0} \times 100 \tag{2}$$

where q_E is the adsorption capacity at equilibrium, RE is the removal efficiency, C_0 is the initial BaP concentration, C_E is the equilibrium concentration of BaP in water after adsorption, V is the volume of solution, and m_{ads} is the adsorbent mass.

This journal is © The Royal Society of Chemistry 2023

Environ. Sci.: Nano, 2023, **10**, 1660–1675 | **1663**

Blanks were performed for all experiments to evaluate the adsorption by the glassware. All experiments were performed in triplicate. The adsorption capacity and removal efficiency were corrected considering the adsorption by the glassware evaluated with the blank experiments. To do so, the concentration adsorbed by the glassware was subtracted from the initial concentration, for the same adsorption time and the same initial aqueous concentration of BaP.

Finally, the reuse and regeneration of FLG@TA@RSN adsorbents were also tested. For this, the adsorption experiments were performed following the same procedure as described above, with 1% ethanol, 10 μg L^{-1} BaP, 5 mg L^{-1} FLG@TA@RSN and 15 min of adsorption time. After magnetic separation, the FG@TA@RSN was washed once with water to remove residual non-adsorbed BaP and magnetic separation was used again to remove all the liquid. Next, desorption was performed, using acetonitrile as extraction solvent. For this, 2 mL of acetonitrile were added to the adsorbent and the mixture was placed in the ultrasound bath for 10 min. Afterwards, the FLG@TA@RSN composites were magnetically separated, and the supernatant was filtered with a 0.20 μm syringe filter and quantified. The FLG@TA@RSN composites were washed, and the adsorption process was repeated. Overall, three cycles of adsorption/desorption were performed. For each recycle, two replicates were performed.

The adsorption removal efficiency was determined for the three cycles. Similarly, the desorption recovery was also determined by the following equation:

$$\text{Recovery} = \frac{m_{\text{desorbed}}}{m_{\text{adsorbed}}} \times 100 = \frac{C_{\text{desorbed}} \times V_{\text{desorption}}}{(C_0 - C_E) \times V_{\text{adsorption}}} \times 100 \quad (3)$$

where m_{desorbed} is the mass desorbed in 10 min using acetonitrile, m_{adsorbed} is the mass adsorbed in 15 min in water with 1% ethanol, C_{desorbed} is the BaP concentration in acetonitrile after desorption, $V_{\text{desorption}}$ is the volume of acetonitrile used in the desorption, C_0 is the initial BaP concentration in the adsorption, C_E is the equilibrium concentration of BaP in water after adsorption, and $V_{\text{adsorption}}$ is the volume of solution in the adsorption.

2.6. Quantification of benzo(*a*)pyrene

To study the adsorption performance of the prepared adsorbents, the BaP still present in solution after adsorption (and desorption) on the synthesized nanomaterials was quantified. BaP was quantified by ultra high-performance liquid chromatography with fluorescence detection (UHPLC-FLD).

The UHPLC system consisted of a Nexera XR model from Shimadzu and was equipped with a Restek Force C$_{18}$ 3 μm 150 × 2.1 mm analytical column and a Restek Force C$_{18}$ 5 μm 5 × 2.1 mm guard column. The detection of BaP was done at optimum excitation/emission wavelengths (290/430 nm)[12] using an RF-20A XS fluorescence detector (Shimadzu).

For the chemical analysis, since BaP was the only species in solution and fluorescence detection is specific, the analytical method was greatly simplified in terms of separation. The mobile phase was 100% methanol, a flow rate of 0.5 mL min^{-1} was used and the oven temperature was set to 30 °C. The injection volume was established at 2 μL and the resulting retention time of BaP in the column was 3.1 min.

A calibration curve (Fig. S2†) was obtained using standard solutions of BaP (0.010 μg L^{-1} to 1000 μg L^{-1}) in acetonitrile and it was performed in triplicate.

When the concentrations were higher than 1000 μg L^{-1}, the samples were diluted to fit the calibration curve range.

The limit of detection (LOD) and limit of quantification (LOQ) were determined based on a signal-to-noise approach. The LOD was considered as the concentration where the signal-to-noise ratio was 3, and in the case of LOQ this ratio was 10. An example of signal and noise determination for LOD and LOQ calculation for the developed method is shown in Fig. S3.† The method established by UHPLC-FLD had a LOD of 4.1 ng L^{-1} (= 0.0041 μg L^{-1}) and a LOQ of 13.7 ng L^{-1} (= 0.0137 μg L^{-1}).

In Fig. S4,† an example of chromatograms following the adsorption process is displayed.

3. Results and discussion

3.1. Characterization of composite adsorbents

3.1.1. Characterization of the synthesized materials. The FLG@TA@RSN CN was successfully synthesized by a one-pot modified polyol solvothermal synthesis method detailed in the Experimental section. The formation of the CNs was confirmed by different characterization techniques and at first by FTIR spectroscopy (Fig. 1(a)). The main difference between the IR spectra of FLG@TA and that of FLG@TA@RSN was the appearance of a band at 580 cm^{-1}, characteristic of the vibration of the Fe–O bond in magnetite[41] as well as an increase of the intensity of bands related to the stretching vibration mode of the C–O bond at ~1080 cm^{-1}, attributed to the presence of residual ethylene glycol in the composite.[36] The remaining bands were present in the spectra of both FLG@TA and FLG@TA@RSN. The band at ~3410 cm^{-1} attributed to the stretching OH vibration could be due to the presence of residual water in the sample as well as to the OH groups of tannic acid and, in the case of FLG@TA@RSN, to the presence of OH groups at the surface of the iron oxide nanostructures. The presence of the band at ~1630 cm^{-1} (vC–O), attributed to aromatic –C–O– of tannic acid, confirmed its presence as well as the bands ~1560 cm^{-1} (vC=C) and ~880 cm^{-1} (δC=C or δC–H). The multiple bands at ~2900 cm^{-1} (vC–H), the band at ~1430 cm^{-1} (δC–H) and the band at ~1380 cm^{-1} (δO–H) could both be due to tannic acid and residual ethylene glycol. Despite the multicomponent composition of the CN with graphene, tannic acid and RSN leading to overlapped IR bands, one may notice that the characteristic aromatic ring breathing vibrations of TA (see Fig. S5†) at 1613 and 1533 cm^{-1} blueshift to 1630 and 1560 cm^{-1}, respectively, and would confirm that TA is adsorbed on graphene layers *via* the π–π interaction between the aromatic
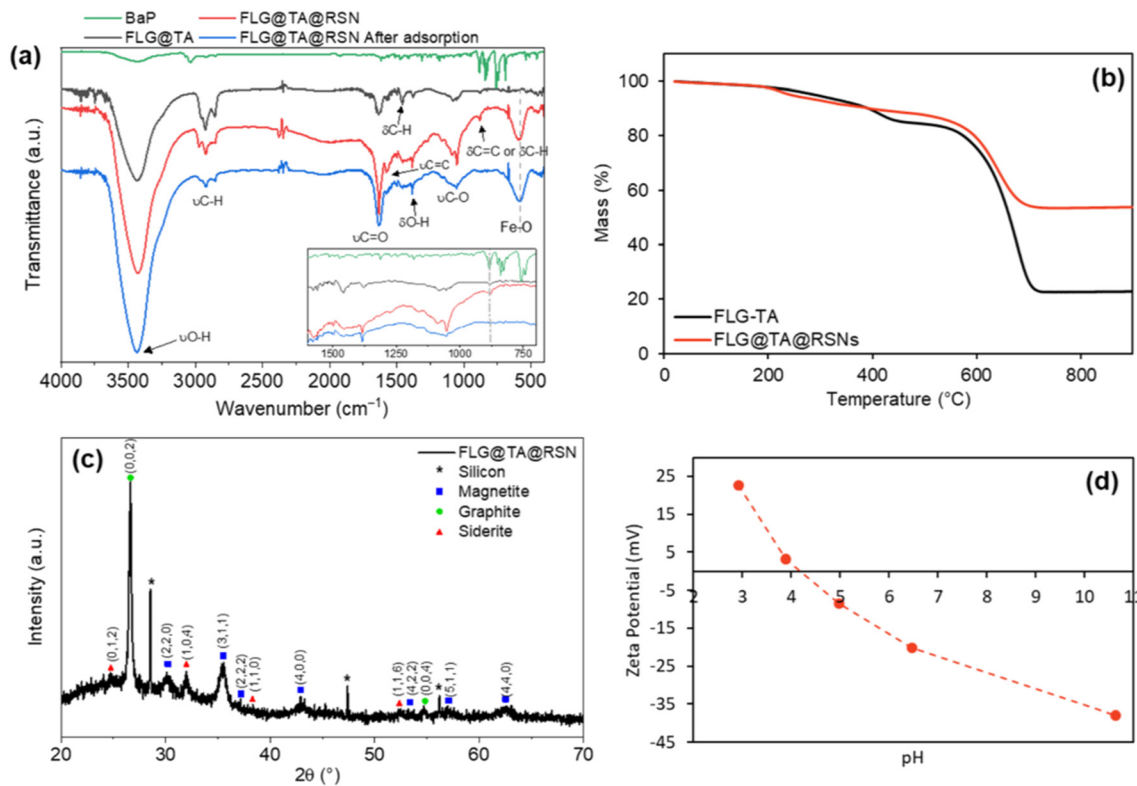
Fig. 1 (a) FTIR spectra where the blue spectrum corresponds to that of FLG@TA@RSN after adsorption with BaP using the concentration of 500 µg L^{-1} BaP in 50% ethanol (inset: zoom in the region between 1600 and 700 cm^{-1}), (b) TGA curves under air, (c) XRD pattern and (d) zeta potential curve as a function of pH of the synthesized CNs.

rings of tannic acid and graphene.[39] A shift is also observed with the O–H stretching vibration (3400 vs. 3430 cm^{-1}) and bending vibration (1317 vs. 1380 cm^{-1}) in agreement with such π–π interactions; however, there is also the contribution of RSN synthesis in these IR bands.

Thermogravimetric analyses under air showed a smaller loss of mass for the composite FLG@TA@RSN in comparison to FLG@TA (Fig. 1(b)). The final mass for FLG@TA was ~23% of its initial mass (indicating a mass loss of ~77%), while for FLG@TA@RSN, the final mass was ~54% of the initial mass (mass loss of ~46%). The lower mass loss for the FLG@TA@RSN was explained by the presence of the iron oxide RSNs in CN that do not decompose in this temperature range. The smallest mass loss in the range 200–400 °C was due to the desorption of chemisorbed water molecules and the burning of tannic acid while the highest mass loss around 600–700 °C was due to graphene combustion.

The presence of both Fe$_{3-x}$O$_4$ and graphite phases in CNs was also confirmed by X-ray diffraction (XRD) (Fig. 1(c)). Here, small characteristic peaks of iron carbonate (FeCO$_3$) were also detected, indicating the formation of this side product during the CN synthesis. Iron carbonate was not observed in TEM and very difficult to observe by SEM, so it is expected that it is present in a very residual quantity and thus it should have no significant influence on the adsorption performance. The crystallite size and lattice parameter of the iron oxide phase were determined by performing profile matching using Fullprof

software. The crystallite size was estimated to be ~9 nm and the lattice parameter of 0.8405 nm corresponded to that of the magnetite phase in such RSNs in agreement with previous studies.[36,37]

The zeta potential curve of FLG@TA@RSN CN aqueous suspension as a function of pH is given in Fig. 1(d). The isoelectric point of the CN was around 4.2. This value was intermediate between the one for graphite (pH 3.2)[42] and the one for magnetite (pH 6–7).[43] The presence of tannic acid in the composite contributed to the lower value of the isoelectric point in comparison to iron oxide, since solutions of tannic acid show negative zeta potential values for pH >1.[44] Thus, the CN suspensions were stable in a large range of pH (above pH ~5).

SEM and TEM images of FLG@TA@RSN (Fig. 2(a, b and d)) show that the iron oxide RSNs were well incorporated within the graphene layers. In Fig. 2(a), it can be seen that the distribution of the RSNs in the composite was homogeneous. Additionally, Fig. 2(b and d) show that the iron oxide RSNs grew around the graphene layers and were strongly anchored on the FLG. This can be observed in more detail in Fig. S6† with higher TEM magnification. The RSN particle size distribution followed a Gaussian distribution (Fig. 2(c)), with an average size of 278 ± 109 nm, which is in agreement with previous studies on the synthesis of iron oxide RSNs by the same polyol solvothermal method, where the average size was 250 ± 12 nm for a reaction time of 13 h.[36] In Fig. 2(e), it

This journal is © The Royal Society of Chemistry 2023

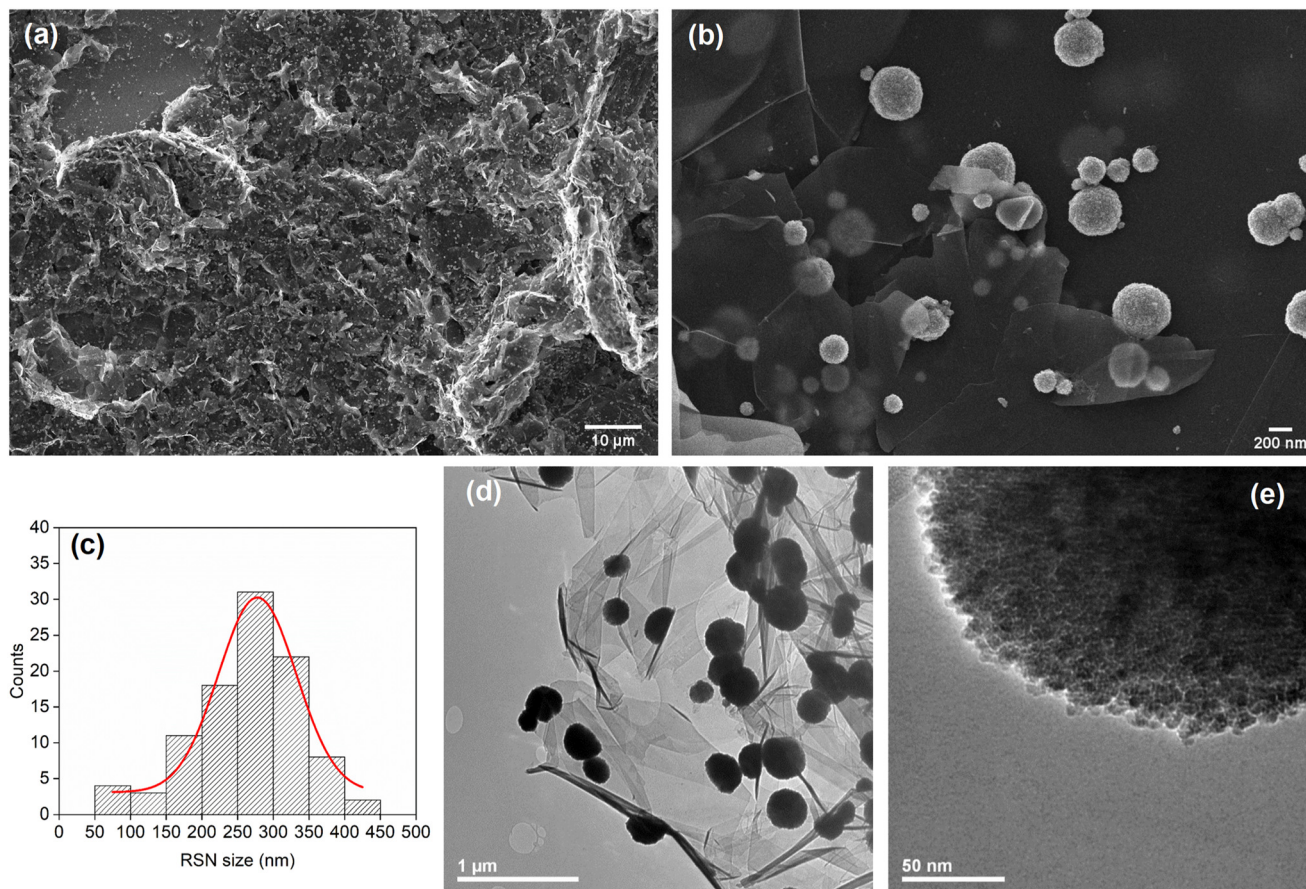Environ. Sci.: Nano, 2023, 10, 1660–1675 | 1665

Fig. 2 SEM (a and b) and TEM (d and e) images of the FLG@TA@RSN adsorbent CNs and (c) histogram size of the iron oxide RSNs in FLG@TA@RSN CNs obtained from TEM images.

is clearly visible that the iron oxide nanostructures in the CNs consisted of aggregates of nanograins. The nanograin size determined from TEM images was in the range 5–11 nm, which is in agreement with the mean crystallite size of ~9 nm calculated from the XRD pattern. The grain size range observed here was smaller than that obtained with RSNs previously synthesized by Gerber *et al.* (25 ± 3 nm).[36] This is explained here by the presence of tannic acid, since lower grain sizes were already reported in other studies due to the presence of this compound.[45]

The specific surface area of the FLG@TA@RSN CNs was also determined to be ~34 m^2 g^{-1}, which is higher than the earlier reported value (27 m^2 g^{-1})[35] due to the smaller grain size and the lower amount of RSN in the CN.

3.1.2. Characterization of CNs after adsorption. After adsorption, CNs with BaP on their surface were analyzed by FTIR spectroscopy to evaluate if any changes in the spectrum could be detected. For this, CNs after adsorption were easily magnetically separated from the supernatant, and CNs resulting from these experiments with a concentration of 500 µg L^{-1} BaP in 50% ethanol were used. Indeed, these conditions led to a higher amount of BaP adsorbed (see section 3.2.2) than in the case of the experiments with 1% ethanol and low BaP concentration in solution. The main

difference observed in the spectra of FLG@TA@RSN before and after adsorption (Fig. 1(a)) was the disappearance of the bands at ~1560 cm^{-1} (vC=C) and ~880 cm^{-1} (δC=C or δC–H). The band at ~880 cm^{-1} is also present in the spectrum of BaP alone. It is expected that BaP can interact with FLG and TA by π–π stacking interactions. Thus, it is possible that these interactions between the aromatic rings of BaP and FLG@TA interfere with the vibration modes of the C=C and C–H bonds in the aromatic rings, leading to the disappearance of these bands. Similar results were reported by Qiao *et al.*, where they studied the adsorption of BaP with biochar and reported that after adsorption the FTIR bands became weaker.[46] There was also a decrease of the intensity of the bands at ~2900 cm^{-1} (vC–H) and of the band at ~1080 cm^{-1} (vC–O), which can also be related to BaP adsorption, but can also possibly be related to desorption of residual ethylene glycol from the CN surface during the adsorption experiment. All of this indicated a modification of the surface chemistry of CNs.

3.2. Adsorption studies of benzo(*a*)pyrene at the surface of CNs

3.2.1. Adsorption of BaP at low concentration in water with 1% ethanol. To study the potential of using the FLG@TA@RSN CNs as adsorbents for the removal of BaP

from water, kinetic experiments were first performed to study how the adsorption evolved as a function of time. As the solubility of BaP in water is quite low,[47] some ethanol was added to water to ensure the solubility of BaP. The amount of ethanol was initially fixed at 1% to remain close to water depollution conditions.

Blank experiments with 1% ethanol had shown that there was a considerable "loss" of BaP certainly due to its sticking to the glassware (Fig. S7†). A constant percentage of 23% of the initial concentration of BaP was deduced according to the linear relationship reported in Fig. S7† between the final and initial concentrations of BaP, suggesting that the BaP adsorption on glass follows the linear range of the Langmuir isotherm. The loss to glassware had been previously noticed for BaP in the work of Qian *et al.*,[40] where it was mentioned that for BaP, even with 10% co-solvent, there can be losses higher than 10% to the glassware. Therefore, all the experiments performed with 1% ethanol presented below were corrected to take into account this BaP glass loss. However, in the case of kinetics experiments, the adsorption

of BaP on the glassware also follows a kinetic model, and thus the contribution of the BaP loss to the glassware was not constant. This means that for shorter times, this contribution was smaller (less loss due to the glassware) than for longer times (more loss due to the glassware). Thus, in the case of a competitive adsorption of BaP by either FLG@TA@RSN or glass, the amount of BaP being potentially adsorbed by FLG@TA@RSN decreased with the increase of adsorption time because there was more adsorption by the glassware. Because of this, the fitting by kinetic models of the obtained data was not possible. Additionally, the residual amount of BaP for all adsorption times was below the LOQ of our chromatographic analytical method, which can also lead to significant quantification errors of residual BaP. Therefore, the kinetic experiments were analysed only in terms of the removal efficiency (determined after correction with the blanks). As can be seen in Fig. 3(a), at an initial concentration of $C_0 = 2.5$ μg L^{-1}, the adsorption of BaP was very fast, with the removal efficiency reaching values higher than ~99% after only 30 s of contact time. This shows that
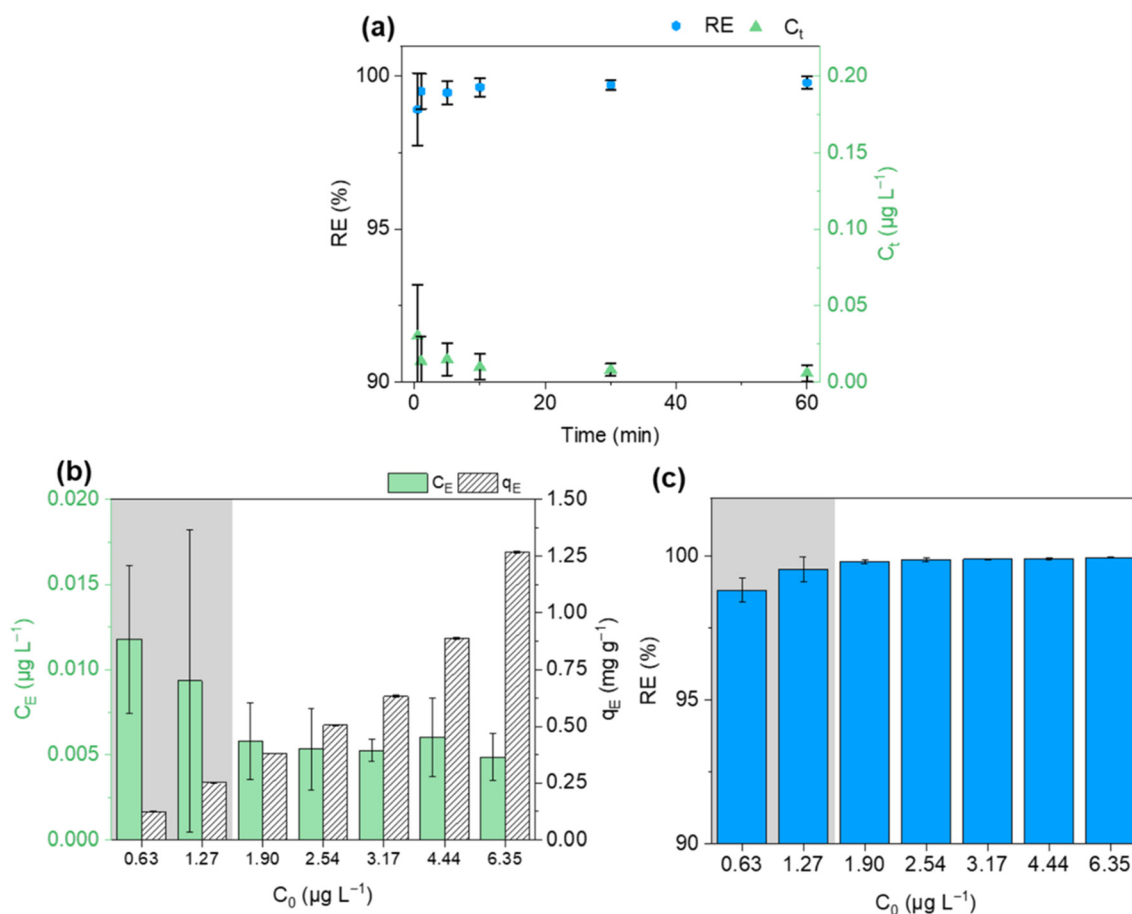

Fig. 3 Adsorption of BaP at room temperature in water in the presence of 1% ethanol: (a) removal efficiency (RE) and concentration after adsorption (C_t) for different adsorption times at an initial concentration of $C_0 = 2.5$ μg L^{-1}; (b) equilibrium concentration (C_E) and adsorption capacity at equilibrium (q_E) for different initial concentrations of BaP; (c) RE for different initial concentrations of BaP. The vertical error bars correspond to the standard deviation determined from triplicates. The grey background indicates experiments performed with C_0 below the water solubility of BaP. Equilibrium concentrations and removal efficiencies were corrected for glassware adsorption based on blank experiments performed (see Fig. S7†).

Table 1 Determined parameters of the Freundlich and Langmuir adsorption isotherm models

		50% ethanol	1% ethanol
Freundlich[a]	K_F ((mg g^{-1}) (L mg^{-1})$^{1/n}$)	38.46 ± 2.48	—[c]
	$1/n$	0.39 ± 0.05	—[c]
	R^2	0.783	—[c]
Langmuir[a]	q_{max} (mg g^{-1})	69.45 ± 5.20	—[c]
	K_L (L mg^{-1})	1.92 ± 0.54	—[c]
	R^2	0.840	—[c]
$q_{E,max}$ (mg g^{-1})[b]		68.13 ± 9.36	1.27 ± 0.01
RE_{max} (%)[b]		31.70 ± 18.59	99.95 ± 0.01

[a] Quoted error bars for the derived parameters correspond to estimates of the standard errors done using the Origin software based on the error propagation formula. [b] Quoted error bars correspond to the standard deviation calculated from the replicate experiments. [c] Isotherm models not determined for 1% ethanol because the determined equilibrium concentration was residual and below the limit of quantification of the developed UHPLC-UV method.

FLG@TA@RSN CNs ensure a very fast and very efficient removal of BaP from water.

When varying the initial BaP concentration in 1% ethanol (Fig. 3(b and c)), it was observed that after one hour of adsorption, the removal efficiencies (Fig. 3(c)) were again very high ($\geq 98.82\%$) whatever the initial concentration of BaP. Indeed, for all studied concentrations, the residual concentration of BaP was below the LOQ of the developed method, so any conclusion related to the values of equilibrium concentration and adsorption capacity must be taken with caution.

In Fig. 3(b), it is visible that the adsorption capacity (q_E) increases with the initial concentration, up to 1.27 mg g^{-1} (Table 1) for the highest C_0. On the other hand, the equilibrium concentration (C_E) of BaP in solution after adsorption is almost constant for all different C_0 values, with the exception of the two smallest values of C_0. It is interesting to note that these two values of C_0 are the only ones below the solubility of BaP in water (1.62 µg L^{-1}),[47] which could be the cause of the slightly different adsorption behavior. At these two lower concentrations, the molecules of BaP might be essentially solvated by water, whereas ethanol will play a role in higher BaP concentrations. Due to these two different

behaviors and the constant C_E values, it was not reasonable to fit any adsorption isotherm models to this set of experimental data.

It is worth noting that in most cases, the concentration of BaP in water after adsorption was below 0.010 µg L^{-1} (Fig. 3(b)), which is the limit established for drinking water by the European Union[16] for BaP alone. Finally, as mentioned in section 2.5., preliminary experiments of adsorption of BaP with a concentration of FLG@TA@RSN of 50 mg L^{-1} were done in addition to the experiments performed with a concentration of 5 mg L^{-1}. In these experiments, after adsorption, no BaP was detected, further confirming the efficiency of the synthesized CNs, when they were present in both lower and higher concentrations.

All these results showed that the synthesized FLG@TA@RSN materials were very efficient in the adsorption of BaP. This indicated there was a strong interaction between BaP and the CNs. It is expected that these interactions corresponded to π–π interactions between the aromatic rings of BaP and the aromatic rings of graphene,[27,31] as illustrated in Fig. 4. It is possible that this type of interactions also occurred between BaP and the aromatic rings present in tannic acid. Tannic acid is also a well-known surfactant of

Fig. 4 Illustration of the interactions between the synthesized CNs and BaP.

iron oxide nanoparticles and could also be present at the surface of RSN, also contributing to the interactions of the CNs with BaP.

3.2.2. Adsorption of BaP at higher concentrations in water with 50% ethanol. In order to be able to study more in depth the adsorption process and because of the impossibility of fitting the adsorption isotherm models to the experimental data obtained with 1% ethanol, the adsorption of BaP in the presence of 50% ethanol/50% water was further studied. With 50% ethanol, higher concentrations of BaP could be used without the limitation of the solubility of BaP in water. This has also allowed evaluating when the adsorption capacity stabilized. More importantly, when 50% ethanol was present, there was no adsorption of BaP by the glassware as highlighted in Fig. S8.†

In Fig. 5(a), the removal efficiencies obtained for different initial concentrations of BaP show that, generally, for low concentrations of BaP, the removal was around 25–35% and then for concentrations higher than 1.5 mg L^{-1}, it decreased with the increase in initial concentration. The adsorption capacity as a function of the equilibrium concentration is presented in Fig. 5(b). The equilibrium adsorption capacity increased with the increase of the equilibrium concentration, and thus with the increase of initial concentration, until it became almost stable for equilibrium concentrations of BaP ≥ 0.75 mg L^{-1}, which corresponds to experiments performed at initial concentration higher than 1 mg L^{-1}.

Two adsorption isotherm models were used to fit the experimental data: Freundlich[17,30,48] and Langmuir.[17,30,49] The fitting was done using the non-linear fitting tool in Origin software. These two models are frequently used and have been employed in other studies such as that performed by Yang *et al.* on the adsorption of BaP.[30]

The Freundlich isotherm is given by the following equation:

$$q_E = K_F C_E^{1/n} \qquad (4)$$

where q_E is the adsorption capacity at equilibrium, C_E is the equilibrium concentration of BaP in water after adsorption, K_F is the Freundlich isotherm constant (in units of (mg g^{-1}) (L mg^{-1})$^{1/n}$) and n is the adsorption intensity.

Similarly, the Langmuir isotherm can be given by:

$$q_E = \frac{q_{max} K_L C_E}{1 + K_L C_E} \qquad (5)$$

where q_{max} is the maximum adsorption capacity (mg g^{-1}) and K_L is the Langmuir isotherm constant (L mg^{-1}).

The fitted Freundlich and Langmuir models are represented in Fig. 5(b) and the derived parameters of the two models as well as the maximum experimental q_E and RE obtained are reported in Table 1.

With both models, the fittings were performed using the concatenate fitting mode for non-linear fitting in Origin software. This mode considers all the replicate data to fit one curve, instead of using just the average values, and thus allowing taking into account the variability of the data for both x (C_E) and y (q_E) values. Looking at the regression coefficient, the model that best fitted to the data was the Langmuir theory isotherm, which had the highest R^2. Similar fittings were observed for many pollutant–adsorbent systems in the literature.[50,51] The R^2 values were not very high because of the fitting taking into account the variability of the replicates. It is important to note that small variations in C_E lead to bigger variations in q_E (see eqn (1)), causing an increase of the standard deviation of this variable.

The Langmuir isotherm assumes that adsorption occurs in a finite number of identical sites on the adsorbent surface and that the adsorption is homogeneous.[17,30] As previously mentioned in the characterization of the FLG@TA@RSN adsorbents, the RSNs were evenly distributed in the graphene layers (Fig. 2(a)), and the composite had a homogeneous surface, supposing the validity of the Langmuir theory and agreeing with the Langmuir isotherm results. The theoretical q_{max} obtained with this model (69.45 ± 5.20 mg g^{-1}) was very

Fig. 5 Adsorption of BaP in 50% water/50% ethanol at room temperature: (a) removal efficiency (RE) for different initial concentrations (C_0) of BaP; (b) experimental adsorption isotherm (q_E *vs.* C_E) fitted with the Langmuir or Freundlich theory. The vertical error bars for RE and q_E and the horizontal error bars for C_E correspond to the standard deviation determined from triplicates. Equilibrium concentrations and removal efficiencies were not corrected since glassware adsorption was negligible under these conditions based on blank experiments performed (Fig. S8†).

Fig. 6 (a) Effect of the ethanol % on the removal efficiency (RE) of BaP for an initial concentration of C_0 = 10 μg L^{-1}; (b) comparison of the RE between FLG@TA@RSN and FLG@TA in 50% water/50% ethanol. The vertical error bars correspond to the standard deviation determined from triplicates in Fig. 5(a) and five replicates in Fig. 5(b). RE values, in the case of the experiments in 1% ethanol, were corrected for glassware adsorption based on blank experiments performed (Fig. S7†). For 50% ethanol, RE values were not corrected since glassware adsorption was negligible (Fig. S8†).

close to the experimental value obtained (68.13 ± 9.36 mg g^{-1}) for the experiments performed in 50% ethanol.

3.2.3. Effect of ethanol content on BaP adsorption. As seen in Fig. 6(a), the presence of ethanol had a clear effect on the adsorption process. An increase of the ethanol content led to a decrease in the removal of BaP by FLG@TA@RSN CNs. At the same BaP concentration of 10 μg L^{-1}, the average removal efficiency in 1% and 10% ethanol was 99.95 ± 0.01% and 95.42 ± 2.31% respectively, while in 50% ethanol, this value was only 31.70 ± 18.59%. This considerable decrease could be due to the fact that in water alone (or at low contents of ethanol), BaP, being highly hydrophobic, had the tendency to prefer to adsorb on the surface of CNs, while in high contents of ethanol, BaP was much more stabilized in solution, certainly because of the much higher solvation effect of ethanol with BaP.

3.2.4. Impact of the presence of RSNs on the CN removal efficiency. The presence of the iron oxide RSNs in the FLG@TA@RSN CNs ensured a very fast and easy magnetic separation of the adsorbent from the depolluted water after adsorption. However, it was important to verify if the presence of RSNs could have a negative impact on the adsorption capacity of the CN itself. This was done by performing adsorption experiments with FLG@TA alone and comparing the results obtained with those obtained with the CNs. Since at 1% ethanol the removal of BaP by the composite was almost total, these experiments were performed in 50% ethanol, where the RE values were lower. As displayed in Fig. 6(b), the presence of RSNs in the composite did not have a negative impact on the removal efficiency. In fact, at lower concentrations of BaP, the composite seems to have an even better performance than FLG@TA alone, although these conclusions should be taken with caution in view of the error bars.

3.2.5. Comparison with adsorption results reported in the literature. Our results were compared with those found in the literature, not only for BaP but also for other PAHs, and are gathered in Table S1† where the adsorption conditions and main results are detailed. For an easier comparison, the main results obtained for the maximum adsorption capacity and the removal efficiency were plotted as a function of adsorbent concentration and as a function of PAH concentration in Fig. 7.

In the present work, the removal of BaP from water (with 1% ethanol to ensure the solubilization of BaP) reached a maximum removal efficiency of 99.95 ± 0.01%, which was obtained with a maximum adsorption capacity of 1.27 ± 0.01 mg g^{-1}, using only a tiny composite adsorbent concentration of 5 mg L^{-1}.

BaP removal from water. First, we can compare the results obtained in this work with those conducted on the adsorption of BaP in water. As shown in Fig. 7, only three previous studies were performed on this highly carcinogenic compound with similar types of adsorbent nanomaterials. By comparing the results obtained in this work to those obtained by Hassan *et al.* with green synthesized iron oxide (Fe_2O_3) nanoparticles,[29] it is visible that our composite is much more efficient. Looking at the q_{max} in their experiments of BaP adsorption, they obtained a value of 0.029 mg g^{-1} for an adsorbent concentration of 90 mg L^{-1}, while our q_{max} value for FLG@TA@RSN was much higher (1.27 mg g^{-1}) for an adsorbent concentration of only 5 mg L^{-1} (Fig. 7(a)), in both cases with similar concentrations of BaP (Fig. 7(b)). Furthermore, with an adsorbent concentration of 10 mg L^{-1} (Fig. 7(c)), the same authors reached 20% removal of BaP,[29] whereas with 5 mg L^{-1} FLG@TA@RSN, our removal efficiencies were higher than 99%. Even when they used higher adsorbent concentrations (90 mg L^{-1} and 130 mg L^{-1} in Fig. 7(c)), the FLG@TA@RSN CN exhibits a better performance.

Similarly, Yang *et al.* used carbon dots/fatty acid-coated magnetic nanoparticles to adsorb BaP with much higher adsorbent concentrations (5 mg L^{-1} *vs.* 180 mg L^{-1}, Fig. 7(a)) and similar BaP concentrations (Fig. 7(b))[30] and obtained much lower adsorption capacity (76.23 × 10^{-3} mg g^{-1} *vs.* 1.27 mg g^{-1}). In terms of removal efficiencies, FLG@TA@RSN also showed better results (Fig. 7(c and d)), highlighting again the high efficiency of this nanocomposite even with a small adsorbent concentration. In fact, for their smallest concentration of adsorbent (30 mg L^{-1}), they obtained removal efficiencies of only 8.4% and 14.7% using fatty acid-coated magnetic nanoparticles and using carbon dots/fatty acid-coated magnetic nanoparticles, respectively,[30] while our removal efficiencies were always higher than 99% with 1% ethanol.

Finally, Adeola and Forbes reported similar adsorption capacity of 1.52 mg g^{-1} for BaP,[32] but they used a concentration of adsorbent (graphene wool) that was 200 times higher than that used in our experiments (Fig. 7(a)). Unfortunately, these authors did not determine any removal efficiency for BaP single-solute experiments.

Other PAH removal from water. It is also possible to compare the synthesized CNs (FLG@TA@RSN), in a more general way, to
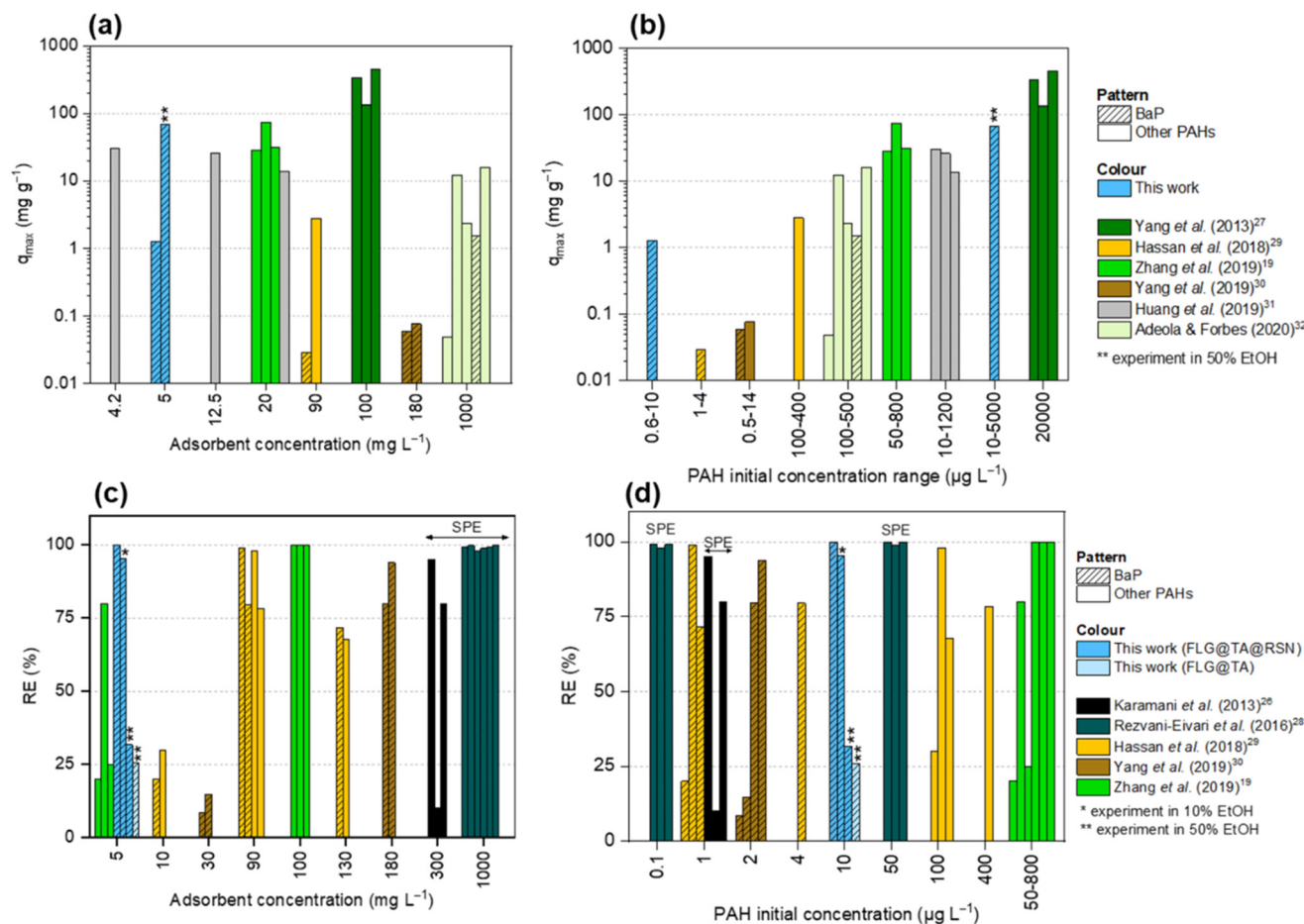
1670 | *Environ. Sci.: Nano*, 2023, **10**, 1660–1675

This journal is © The Royal Society of Chemistry 2023

Fig. 7 Comparison of this work with other published results in the literature[19,26–32] in terms of (a) q_{max} as a function of the adsorbent concentration, (b) q_{max} as a function of the PAH initial concentration range, (c) RE as a function of the adsorbent concentration, and (d) RE as a function of the PAH initial concentration range. SPE indicates studies where solid-phase extraction was used instead of batch adsorption experiments. This work was performed in water with 1% ethanol, 10% ethanol (*) and 50% ethanol (**).

other magnetic carbon-based composites used for the adsorption of other PAHs in water media. Magnetic carbon nanotubes and magnetic graphene sheets were used by Zhang *et al.* to adsorb phenanthrene (PHE) and much higher adsorption capacities were obtained by them in comparison to our experiments or removal of BaP from water (with 1% ethanol).[19] However, in their work, possibly because PHE has a higher solubility in water, much higher concentrations of PHE were used, which led to higher adsorption capacities (see eqn (1) in section 2.5). In fact, if we compare their results with the experiments performed with FLG@TA@RSN in 50% ethanol, where much higher concentrations of BaP were used (Fig. 7(b)), we observe that the adsorption capacities were in the same range (68.13 mg g^{-1} for FLG@TA@RSN *vs.* 20.0–74.61 mg g^{-1} in their work depending on the adsorbent material).[19] It is also worth noting that again, these authors used a higher adsorbent concentration (20 mg L^{-1}) in comparison to the FLG@TA@RSN ones we used in our experiments (Fig. 7(a)). Moreover, when using a similar concentration of adsorbent (5 mg L^{-1}) (Fig. 7(c)), they obtained a much lower removal of PHE ($\leq$80% *vs.* 99.95% in our case).

Similarly, Huang *et al.* also studied the adsorption of PHE with magnetic graphene oxide and magnetic reduced graphene[31] for similar or higher concentrations of adsorbent and similar concentrations of PHE to our experiments with BaP in 50% ethanol. In their work, q_{max} values ranging between 13.6 and 30.1 mg g^{-1} were obtained, which were lower than the one of 68.13 mg g^{-1} obtained with FLG@TA@RSN (Fig. 7(a and b)).

Finally, concerning the batch experiments, Yang *et al.* studied the adsorption of naphthalene (NAP) and obtained higher adsorption capacities of 73 up to 636 mg g^{-1}.[27] This big difference can be related mainly to the much higher initial NAP concentration used (20 000 µg L^{-1}, Fig. 7(b)). Again, these high concentrations could be used because of the high solubility of naphthalene in water (31 mg L^{-1}).[27]

In Fig. 7(c and d), the studies of Rezvani-Eivari *et al.*[28] and Karamani *et al.*[26] are also displayed. Instead of batch experiments, they used their magnetic carbon-based materials to depollute water containing PAHs, similarly to that done with solid-phase extraction (SPE) cartridges. They determined the capacity of their materials to retain the

pollutant in terms of the recovery, which corresponds to the amount of pollutant in solution after desorption of the used adsorbent divided by the initial amount of pollutant in solution. Rezvani-Eivari *et al.* studied the extraction of NAP, PHE and fluorene (FLU) from water,[28] while Karamani *et al.* studied the extraction of the 16 priority EPA PAHs.[26] It is possible to compare the removal efficiencies obtained with FLG@TA@RSN with the recoveries obtained by SPE and considering the PAH initial concentrations, we can then compare these studies to our experiments performed in water with 1% ethanol. Again, the potential of FLG@TA@RSN for the removal of PAHs from water is clearly highlighted, since the removal efficiency of BaP was similar or, in most cases, higher than the recoveries obtained by Rezvani-Eivari *et al.* and Karamani *et al.*, where they used a much higher amount of solid adsorbent (20 mg for 20 mL of solution,[28] corresponding to 1000 mg L^{-1}, and 15 mg for 50 mL of solution,[26] thus 300 mg L^{-1}, respectively).

Given the small amount of material used in our experiments compared to those reported in the literature, it results that our synthesized CNs are very efficient for the adsorption of benzo(*a*)pyrene.

3.2.6. Reuse and regeneration of the FLG@TA@RSN adsorbents. The reuse and regeneration of FLG@TA@RSN as adsorbent were assessed by doing three cycles of adsorption/ desorption for two replicates. The obtained results are presented in Fig. 8.

In the first adsorption cycle, the RE value was 95.85 ± 1.03%. This was slightly lower than the maximum adsorption efficiency of 99.95 ± 0.01% obtained after 1 hour (see Table 1
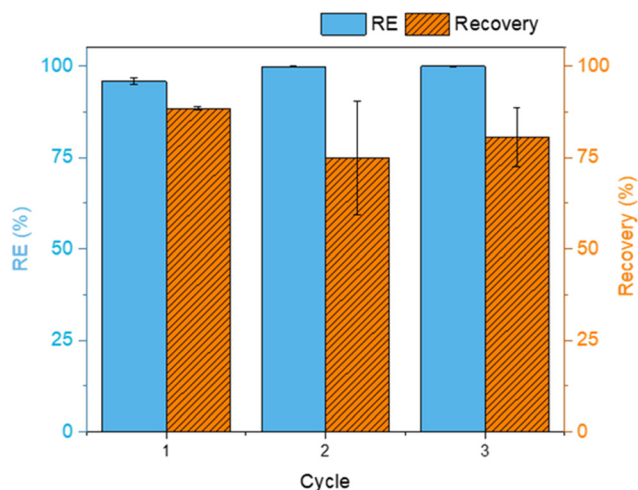
and Fig. 5(a)), which was due to the fact that the recycling adsorption time was only 15 min. For the first desorption cycle, a recovery of 88.48 ± 0.46% was obtained with acetonitrile as extraction solvent. There was no total recovery of BaP, but this did not seem to be prejudicial for the adsorption of BaP in the following cycles. In fact, the adsorption of BaP increased to 99.89 ± 0.15% and to 99.17 ± 0.03% in cycles 2 and 3, respectively. The residual amount of BaP on the adsorbent surface might promote the adsorption by π–π interactions between the adsorbed BaP and the BaP in solution.

For the desorption process, the recovery decreased to about 12% after cycle 1. However, the standard deviation was higher, so it was not easy to conclude. Nevertheless, this lower recovery does not have a negative effect on the adsorption performance of the FLG@TA@RSN CNs. A higher number of reuse/regeneration cycles should be tested in the future, but the obtained results are promising, showing that the CNs have good reusability.

4. Conclusions

In this work, a magnetic few-layer graphene nanocomposite adsorbent was successfully synthesized and was demonstrated to be highly efficient for the removal of benzo(*a*)pyrene, a highly carcinogenic PAH. The synthesis of the composite nanomaterial by adding FLG@TA to the reaction mixture of iron oxide RSNs was reproducible and led to homogeneously distributed iron oxide nanostructures on the graphene layers. The magnetic properties provided by RSNs allowed a quick magnetic separation of the adsorbent from the supernatant. In addition, the presence of RSNs in CNs did not affect the adsorption capacity of FLG@TA.

CNs were shown to be very effective for the removal of BaP from water, with removal of almost all BaP in solution after only 30 seconds. Moreover, when varying the initial concentration of BaP up to 10 µg L^{-1}, the FLG@TA@RSN had removal efficiencies of above 98.82% for all studied cases, reaching a maximum removal of 99.95%. The concentration of BaP in water after adsorption was generally below 10 ng L^{-1}, which is the limit established for drinking water by the European Union. Thus, this shows the potential of CNs for water depollution of BaP, allowing compliance with the existing directives.[16]

It was also concluded that the presence of a co-solvent, here ethanol, in high amounts can limit the adsorption of BaP. However, in small quantities (1–10%), it did not hinder the adsorption of BaP and ensures its solubilization.

The concentration of FLG@TA@RSN used for adsorption experiments of BaP was quite low (5 mg L^{-1}) in comparison to other studies in the literature but did not compromise the removal efficiency. Thus, overall, the as-prepared magnetic few-layer graphene CNs are very promising for the removal of BaP from water and will potentially also be efficient in the removal of other dangerous PAHs or other persistent organic pollutants (POPs).

Fig. 8 Adsorption removal efficiency (blue) and desorption recovery (orange) for three cycles of regeneration of FLG@TA@RSN adsorbent. For adsorption, a BaP aqueous solution of 10 µg L^{-1} was prepared with 1% ethanol. An adsorption experiment was performed using 5 mg L^{-1} CN adsorbent for 15 min. For desorption, 2 mL of acetonitrile was used and desorption was performed for 10 min in an ultrasound bath. The vertical error bars correspond to the standard deviation determined from the two replicates. The removal efficiencies of the adsorption experiments were corrected for glassware adsorption based on blank experiments performed (see Fig. S7†).

1672 | *Environ. Sci.: Nano*, 2023, **10**, 1660–1675

This journal is © The Royal Society of Chemistry 2023

Following the high efficiency of BaP removal of the synthesized FLG@TA@RSN CNs, it would be important in the future to develop methodologies to integrate these nanocomposites in standard large-scale depollution practices without compromising their efficiency as well as their magnetic properties.

Conflicts of interest

The authors declare no conflicts of interest.

Acknowledgements

References

1 H. Borji, G. M. Ayoub, M. Al-Hindi, L. Malaeb and H. Z. Hamdan, Nanotechnology to remove polychlorinated biphenyls and polycyclic aromatic hydrocarbons from water: a review, *Environ. Chem. Lett.*, 2020, **18**, 729–746.

2 S. J. Tesh and T. B. Scott, Nano-Composites for Water Remediation: A Review, *Adv. Mater.*, 2014, **26**, 6056–6068.

3 A. M. Awad, R. Jalab, A. Benamor, M. S. Nasser, M. M. Ba-Abbad, M. El-Naas and A. W. Mohammad, Adsorption of organic pollutants by nanomaterial-based adsorbents: An overview, *J. Mol. Liq.*, 2020, **301**, 112335.

4 M. N. Rashed, in *Organic Pollutants*, IntechOpen, Rijeka, 2013, ch. 7.

5 M. M. Paixão, M. T. G. Vianna and M. Marques, Graphene and graphene nanocomposites for the removal of aromatic organic compounds from the water: systematic review, *Mater. Res. Express*, 2018, **5**, 012002.

6 A. Mojiri, J. L. Zhou, A. Ohashi, N. Ozaki and T. Kindaichi, Comprehensive review of polycyclic aromatic hydrocarbons in water sources, their effects and treatments, *Sci. Total Environ.*, 2019, **696**, 133971.

7 F. R. Nursanto, J. Vaz-Ramos, O. Delhomme, S. Bégin-Colin and S. Le Calvé, Simultaneous Monitoring of Outdoor PAHs and Particles in a French Peri-Urban Site during COVID Restrictions and the Winter Saharan Dust Event, *Atmosphere*, 2022, **13**, 1435.

8 W. Wilcke, Global patterns of polycyclic aromatic hydrocarbons (PAHs) in soil, *Geoderma*, 2007, **141**, 157–166.

9 H. I. Abdel-Shafy and M. S. M. Mansour, A review on polycyclic aromatic hydrocarbons: Source, environmental impact, effect on human health and remediation, *Egypt. J. Pet.*, 2016, **25**, 107–123.

10 L. Zhang, L. Yang, Q. Zhou, X. Zhang, W. Xing, Y. Wei, M. Hu, L. Zhao, A. Toriba, K. Hayakawa and N. Tang, Size distribution of particulate polycyclic aromatic hydrocarbons in fresh combustion smoke and ambient air: A review, *J. Environ. Sci.*, 2020, **88**, 370–384.

11 C. Liaud, T. Dintzer, V. Tschamber, G. Trouve and S. Le Calvé, Particle-bound PAHs quantification using a 3-stages cascade impactor in French indoor environments, *Environ. Pollut.*, 2014, **195**, 64–72.

12 C. Liaud, S. Chouvenc and S. Le Calvé, Simultaneous Monitoring of Particle-Bound PAHs Inside a Low-Energy School Building and Outdoors over Two Weeks in France, *Atmosphere*, 2021, **12**, 108.

13 M. Dimashki, L. H. Lim, R. M. Harrison and S. Harrad, Temporal Trends, Temperature Dependence, and Relative Reactivity of Atmospheric Polycyclic Aromatic Hydrocarbons, *Environ. Sci. Technol.*, 2001, **35**, 2264–2267.

14 G. K. Gaurav, T. Mehmood, M. Kumar, L. Cheng, K. Sathishkumar, A. Kumar and D. Yadav, Review on polycyclic aromatic hydrocarbons (PAHs) migration from wastewater, *J. Contam. Hydrol.*, 2021, **236**, 103715.

15 S. Lamichhane, K. C. Bal Krishna and R. Sarukkalige, Polycyclic aromatic hydrocarbons (PAHs) removal by sorption: A review, *Chemosphere*, 2016, **148**, 336–353.

16 European Commission, Directive (EU) 2020/2184 of the European Parliament and of the Council of 16 December 2020 on the quality of water intended for human consumption (recast), *Off. J. Eur. Union L*, 2020, **435**, 1–62.

17 K. Y. Foo and B. H. Hameed, Insights into the modeling of adsorption isotherm systems, *Chem. Eng. J.*, 2010, **156**, 2–10.

18 B. Sun, Q. Li, M. Zheng, G. Su, S. Lin, M. Wu, C. Li, Q. Wang, Y. Tao, L. Dai, Y. Qin and B. Meng, Recent advances in the removal of persistent organic pollutants (POPs) using multifunctional materials:a review, *Environ. Pollut.*, 2020, **265**, 114908.

19 J. Zhang, R. Li, G. Ding, Y. Wang and C. Wang, Sorptive removal of phenanthrene from water by magnetic carbon nanomaterials, *J. Mol. Liq.*, 2019, **293**, 111540.

20 Y. Li, C. Zhao, Y. Wen, Y. Wang and Y. Yang, Adsorption performance and mechanism of magnetic reduced graphene oxide in glyphosate contaminated water, *Environ. Sci. Pollut. Res.*, 2018, **25**, 21036–21048.

21 K. Shrivas, A. Ghosale, N. Nirmalkar, A. Srivastava, S. K. Singh and S. S. Shinde, Removal of endrin and dieldrin isomeric pesticides through stereoselective adsorption behavior on the graphene oxide-magnetic nanoparticles, *Environ. Sci. Pollut. Res.*, 2017, **24**, 24980–24988.

22 H. Abdolmohammad-Zadeh, A. Zamani and Z. Shamsi, Extraction of four endocrine-disrupting chemicals using a Fe3O4/graphene oxide/di-(2-ethylhexyl) phosphoric acid nano-composite, and their quantification by HPLC-UV, *Microchem. J.*, 2020, **157**, 104964.

23 K. Ouyang, C. Zhu, Y. Zhao, L. Wang, S. Xie and Q. Wang, Adsorption mechanism of magnetically separable Fe3O4/

This journal is © The Royal Society of Chemistry 2023

Environ. Sci.: Nano, 2023, **10**, 1660–1675 | 1673

graphene oxide hybrids, *Appl. Surf. Sci.*, 2015, **355**, 562–569.

24 L. Vidal, M. Ahmadi, E. Fernández, T. Madrakian and A. Canals, Magnetic headspace adsorptive extraction of chlorobenzenes prior to thermal desorption gas chromatography-mass spectrometry, *Anal. Chim. Acta*, 2017, **971**, 40–47.

25 S. Zeng, N. Gan, R. Weideman-Mera, Y. Cao, T. Li and W. Sang, Enrichment of polychlorinated biphenyl 28 from aqueous solutions using Fe3O4 grafted graphene oxide, *Chem. Eng. J.*, 2013, **218**, 108–115.

26 A. A. Karamani, A. P. Douvalis and C. D. Stalikas, Zero-valent iron/iron oxide-oxyhydroxide/graphene as a magnetic sorbent for the enrichment of polychlorinated biphenyls, polyaromatic hydrocarbons and phthalates prior to gas chromatography–mass spectrometry, *J. Chromatogr. A*, 2013, **1271**, 1–9.

27 X. Yang, J. Li, T. Wen, X. Ren, Y. Huang and X. Wang, Adsorption of naphthalene and its derivatives on magnetic graphene composites and the mechanism investigation, *Colloids Surf., A*, 2013, **422**, 118–125.

28 M. Rezvani-Eivari, A. Amiri, M. Baghayeri and F. Ghaemi, Magnetized graphene layers synthesized on the carbon nanofibers as novel adsorbent for the extraction of polycyclic aromatic hydrocarbons from environmental water samples, *J. Chromatogr. A*, 2016, **1465**, 1–8.

29 S. S. M. Hassan, H. I. Abdel-Shafy and M. S. M. Mansour, Removal of pyrene and benzo(a)pyrene micropollutant from water via adsorption by green synthesized iron oxide nanoparticles, *Adv. Nat. Sci.: Nanosci. Nanotechnol.*, 2018, **9**, 015006.

30 D. Yang, S. K. Tammina, X. Li and Y. Yang, Enhanced removal and detection of benzo[a]pyrene in environmental water samples using carbon dots-modified magnetic nanocomposites, *Ecotoxicol. Environ. Saf.*, 2019, **170**, 383–390.

31 D. Huang, B. Xu, J. Wu, P. C. Brookes and J. Xu, Adsorption and desorption of phenanthrene by magnetic graphene nanomaterials from water: Roles of pH, heavy metal ions and natural organic matter, *Chem. Eng. J.*, 2019, **368**, 390–399.

32 A. O. Adeola and P. B. C. Forbes, Assessment of reusable graphene wool adsorbent for the simultaneous removal of selected 2–6 ringed polycyclic aromatic hydrocarbons from aqueous solution, *Environ. Technol.*, 2020, 1–14.

33 S. Hamze, N. Berrada, D. Cabaleiro, A. Desforges, J. Ghanbaja, J. Gleize, D. Bégin, F. Michaux, T. Maré, B. Vigolo and P. Estellé, Few-Layer Graphene-Based Nanofluids with Enhanced Thermal Conductivity, *Nanomaterials*, 2020, **10**, 1258.

34 E. Pardieu, S. Pronkin, M. Dolci, T. Dintzer, B. P. Pichon, D. Begin, C. Pham-Huu, P. Schaaf, S. Begin-Colin and F. Boulmedais, Hybrid layer-by-layer composites based on a conducting polyelectrolyte and Fe3O4 nanostructures grafted onto graphene for supercapacitor application, *J. Mater. Chem. A*, 2015, **3**, 22877–22885.

35 O. Gerber, S. Bégin-Colin, B. P. Pichon, E. Barraud, S. Lemonnier, C. Pham-Huu, B. Daffos, P. Simon, J. Come and D. Bégin, Design of Fe3–xO4 raspberry decorated graphene nanocomposites with high performances in lithium-ion battery, *J. Energy Chem.*, 2016, **25**, 272–277.

36 O. Gerber, B. P. Pichon, D. Ihiawakrim, I. Florea, S. Moldovan, O. Ersen, D. Begin, J.-M. Grenèche, S. Lemonnier, E. Barraud and S. Begin-Colin, Synthesis engineering of iron oxide raspberry-shaped nanostructures, *Nanoscale*, 2017, **9**, 305–313.

37 O. Gerber, B. P. Pichon, C. Ulhaq, J.-M. Grenèche, C. Lefevre, I. Florea, O. Ersen, D. Begin, S. Lemonnier, E. Barraud and S. Begin-Colin, Low Oxidation State and Enhanced Magnetic Properties Induced by Raspberry Shaped Nanostructures of Iron Oxide, *J. Phys. Chem. C*, 2015, **119**, 24665–24673.

38 Z. Yu, Z. Shi, H. Xu, X. Ma, M. Tian and J. Yin, Green chemistry: Co-assembly of tannin-assisted exfoliated low-defect graphene and epoxy natural rubber latex to form soft and elastic nacre-like film with good electrical conductivity, *Carbon*, 2017, **114**, 649–660.

39 S. Zhao, S. Xie, Z. Zhao, J. Zhang, L. Li and Z. Xin, Green and High-Efficiency Production of Graphene by Tannic Acid-Assisted Exfoliation of Graphite in Water, *ACS Sustainable Chem. Eng.*, 2018, **6**, 7652–7661.

40 Y. Qian, T. Posch and T. C. Schmidt, Sorption of polycyclic aromatic hydrocarbons (PAHs) on glass surfaces, *Chemosphere*, 2011, **82**, 859–865.

41 M. Veneranda, J. Aramendia, L. Bellot-Gurlet, P. Colomban, K. Castro and J. M. Madariaga, FTIR spectroscopic semi-quantification of iron phases: A new method to evaluate the protection ability index (PAI) of archaeological artefacts corrosion systems, *Corros. Sci.*, 2018, **133**, 68–77.

42 A. Barišić, J. Lützenkirchen, N. Bebić, Q. Li, K. Hanna, A. Shchukarev and T. Begović, Experimental Data Contributing to the Elusive Surface Charge of Inert Materials in Contact with Aqueous Media, *Colloids Interfaces*, 2021, **5**, 6.

43 M. Kosmulski, The pH dependent surface charging and points of zero charge. IX. Update, *Adv. Colloid Interface Sci.*, 2021, **296**, 102519.

44 S. Dultz, R. Mikutta, S. N. M. Kara, S. K. Woche and G. Guggenberger, Effects of solution chemistry on conformation of self-aggregated tannic acid revealed by laser light scattering, *Sci. Total Environ.*, 2021, **754**, 142119.

45 C. Hou, Y. Wang, H. Zhu and H. Wei, Preparation of mesopourous Fe3O4 nanoparticle with template reagent: Tannic acid and the catalytic performance, *J. Taiwan Inst. Chem. Eng.*, 2016, **60**, 438–444.

46 K. Qiao, W. Tian, J. Bai, J. Dong, J. Zhao, X. Gong and S. Liu, Preparation of biochar from Enteromorpha prolifera and its use for the removal of polycyclic aromatic hydrocarbons (PAHs) from aqueous solution, *Ecotoxicol. Environ. Saf.*, 2018, **149**, 80–87.

47 W. E. May, S. P. Wasik, M. M. Miller, Y. B. Tewari, J. M. Brown-Thomas and R. N. Goldberg, Solution thermodynamics of some slightly soluble hydrocarbons in water, *J. Chem. Eng. Data*, 1983, **28**, 197–200.

1674 | *Environ. Sci.: Nano*, 2023, **10**, 1660–1675

This journal is © The Royal Society of Chemistry 2023

48 H. M. F. Freundlich, Over the adsorption in solution, *J. Phys. Chem.*, 1906, **57**, 385–471.

49 I. Langmuir, The constitution and fundamental properties of solids and liquids, *J. Am. Chem. Soc.*, 1916, **38**, 2221–2295.

50 O. Duman, C. Özcan, T. Gürkan Polat and S. Tunç, Carbon nanotube-based magnetic and non-magnetic adsorbents for the high-efficiency removal of diquat dibromide herbicide from water: OMWCNT, OMWCNT-Fe3O4 and OMWCNT-κ-carrageenan-Fe3O4 nanocomposites, *Environ. Pollut.*, 2019, **244**, 723–732.

51 O. Duman, T. G. Polat and S. Tunç, Development of poly(vinyl alcohol)/β-cyclodextrin/P(MVE-MA) composite nanofibers as effective and selective adsorbent and filtration material for the removal and separation of cationic dyes from water, *J. Environ. Manage.*, 2022, **322**, 116130.

This journal is © The Royal Society of Chemistry 2023

Environ. Sci.: Nano, 2023, **10**, 1660–1675 | **1675**